Recent progress in modelling the resolution and localization of Doppler reflectometry measurements

G.D.Conway[1], C.Lechte[2], E.Poli[1], O.Maj[1] and the ASDEX Upgrade Team

[1]*Max-Planck Institut für Plasmaphysik, Garching 85748, Germany*
[2]*Inst. Interfacial Proc. Eng. & Plasma Tech., Uni. Stuttgart, Germany*

1. Introduction

Doppler reflectometry/backscatter is an established mm-wave technique in magnetic confinement devices for measuring plasma turbulence characteristics - such as the propagation velocity $u_\perp = \omega_D/k_\perp$ from the backscatter signal Doppler shift ω_D, the turbulence structure and $k_\perp$ wavenumber spectrum from multi-probing spatial correlations. Current analysis techniques employ beam/ray-tracing methods - with experimental n_e density profiles and flux surface equilibria (i.e. non-planar cutoff layers) - to give the measurement radial location r and the probed turbulence perpendicular (i.e. binormal) wavenumber $k_\perp = -2N_\perp k_0$ where $N_\perp$ is the perpendicular component of the refractive index at the beam/ray turning point (tp). The error bars Δr and $\Delta k_\perp$ are often estimated from analytic formulas. An initial benchmarking of these parameters using 2D full-wave simulations was performed for an (upper) Xu-mode beam propagation in ASDEX Upgrade (AUG) geometry [1]. Here, this study is extended with ne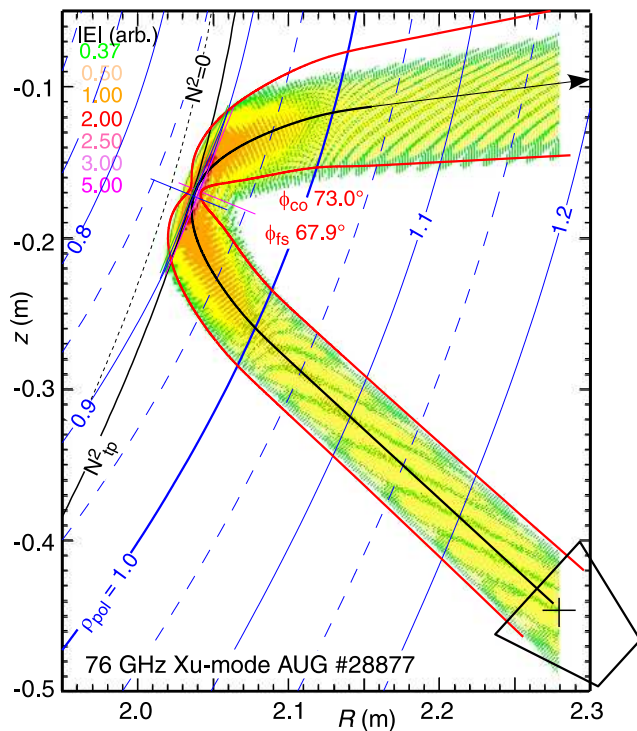w simulation scans with different densities, plasma shape, antenna tilt angles, as well as O-mode, and for the first time (lower) Xl-mode probing.

2. Simulation approach

As in the previous study the approach is to model a series of real AUG L-mode discharges with experimental CLISTE equilibria and fitted (mTanh) n_e profiles, and a geometry based on the V-band Doppler reflectometer [2]. Full-wave simulations are made using the X-mode capable IPF-FD3D finite difference time domain code operating in 2D geometry [3]. The actual reflectometer bistatic hog-horn antennas are modelled as monostatic Gaussian beams with comparable beam divergences. The code outputs the absolute wave electric field $|E|$ and the complex weighting function $W(\boldsymbol{r})$ on a $r-z$ grid.

Fig. 1: *Full-wave $|E|$ contours with ray (black) & beam-trace envelope (red) for X-mode 76 GHz. Flux surfaces (blue) and N_{tp}^2 cutoff layer (black).*

1

Fig. 1 shows an example 2D snap-shot of $|E|$ contours for a 76 GHz, Xu-mode beam in AUG lower-single-null, low density shot #28877. The outer contour (green) is the launched $E_{1/e}$ wave-amplitude. The antenna is outside the plasma. Overlaid is the central ray (black) from the TORBEAM code [4], plus the beam-trace (local) $E_{1/e}$ envelope (red), which tracks the vacuum full-wave, but diverges in plasma as the axis E changes.

A dataset of 42 simulation runs is formed from 3 shots (#28877, #27969 LSN and #33953 circ. limiter) at low: $n_{e0} = 2.9$ and high: 8.6×10^{19} m^{-3} core density, $B_T = -2.4$ T with multiple frequency scans in O, Xu and Xl-mode covering SOL, edge and core radii, plus antenna tilt and beam divergence scans.

3. Weighting function

The backscattered beam results primarily from the turbulence interaction with the incident beam around the turning point. Thus, the spatial structure of the wave $|E|$ field determines the backscatter location and the wavenumber sensitivity - as exploited in previous studies [1]. However, a more precise approach is to examine the time-independent wave spatial complex Weighting function $W(\boldsymbol{r}) = \langle E_i(\boldsymbol{r}, t) E_a(\boldsymbol{r}, t) \rangle$ (computed in the full-wave code, on the same Cartesian grid, as the product of the incident E_i and antenna E_a beam averaged over one wave period) [5]. The receiver signal (within the Born limit) $I^2(t) = (\eta \int \delta n(\boldsymbol{r}, t) W(\boldsymbol{r}) d\boldsymbol{r})^2 \propto Pow(E^2)$ is obtained by spatially integrating W weighted with the density fluctuation $\delta n(t)$ [6]. This analysis has also been performed for the dataset, but is not presented here. Without turbulence (ideal case) the spatial structure of $W \propto E^2$ gives all the necessary information on the beam interaction zone [5].
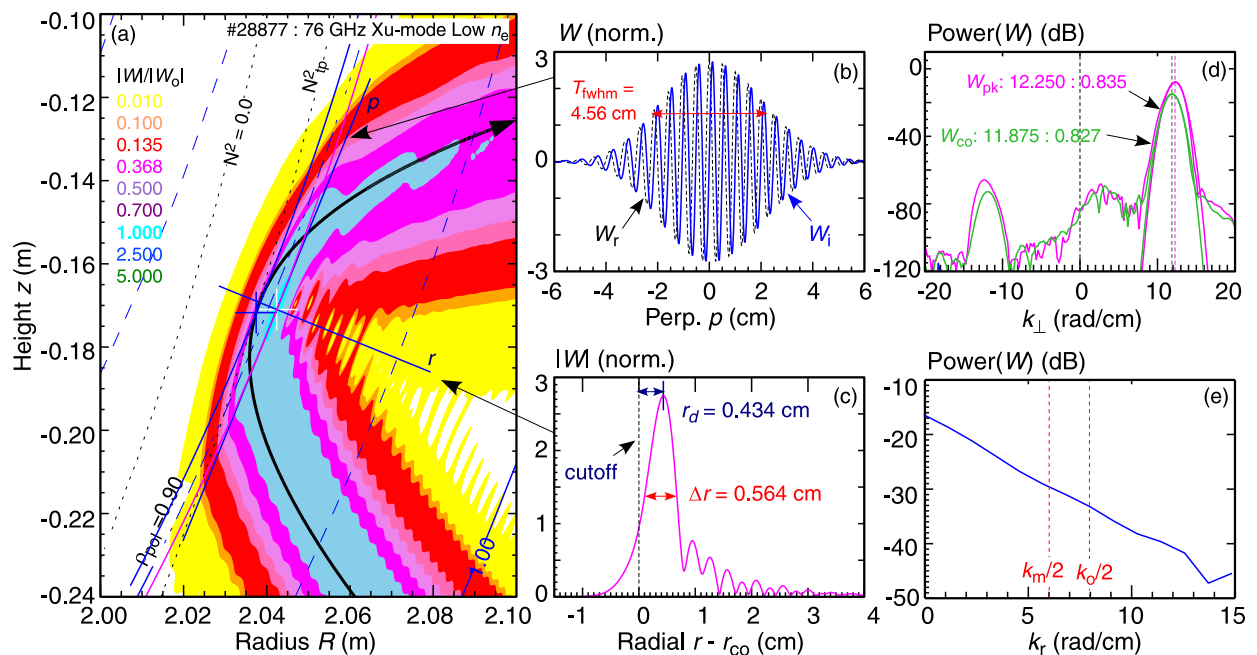

Fig. 2: (a) Normalized full-wave $|W/W_0|$ plus (b) tangential & (c) normal slices to cutoff through W_{pk} with (d) corresponding $k_\perp$ and k_r power spectra for 76 GHz, Xu-mode, low n_e #28877.

2

Fig. 2(a) shows a zoom of $|W|$ contours normalized to launch $|W_0|$ for the fig. 1 case, with slices through the maxima $|W|_{pk}$ (not the ray-tp). which are (b) tangential and (c) normal to the cutoff layer. Here the term cutoff is used to mean the position where the beam group velocity changes sign, i.e. where $N^2 \to$ minimum for the oblique incidence, rather than the position where $N^2 = 0$. Along the tangential (e.g. binormal or perp. direction) the real and imaginary components W_r and W_i are sinusoids with a Gaussian envelope - the width of which is the beam fwhm spot size T. The corresponding power spectrum $Pow(W)$ in fig. 2(d) gives the peak wavenumber $k_\perp$ and the 3dB (fwhm) receiver spectral width $\Delta k_\perp$.

Along the normal (e.g. radial) $|W|$ has the form of a (squared) Airy integral function $Ai^2(r)$ with a last lobe peak displacement r_d from the cutoff and (fwhm) width Δr. The corresponding k_r power spectral (e) is broad and featureless. The Ai^2 form, observed in both 1D perpendicular incidence [7] and 2D non-perpendicular incidence Doppler simulations [8, 1], is not unexpected for fields near a fold caustic [9].

Fig. 3: *Airy fnct. Ai criterion $|\nabla k^2|^{1/3}(r - r_{co})$ vs probing wavenumber $k_\perp$ for dataset.*

4. Bananas & Mirrors

Fig. 1 is an example of core plasma probing at shallow tilt angles where the beam bends before reaching the cutoff surface, cf. squared refractive index $N^2 = \epsilon$ contour at the ray-tp, to form a banana-like path with clear separation of the incoming and reflected beams. For edge probing or steep tilt angles the ray-tp is sharp and the beams overlap forming a mirror-like reflection and an interference pattern. The transition is determined principally by the refractive index radial gradient in the form $|\na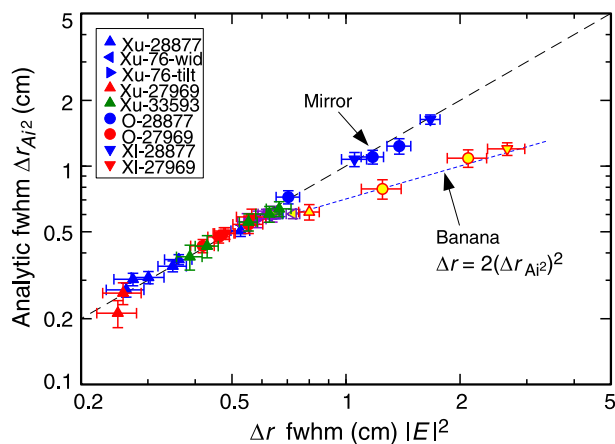bla_r k^2|^{1/3}(r - r_{co}) < 5$, which defines when the linear approximation for $k^2 = N^2 k_0^2$ near the cutoff is no longer accurate in the wave solution [7]. This is plotted in fig. 3 vs probing $k_\perp$ for the database with the distance $(r - r_{co}) = r_{Ai1}$ (see below). For points < 5 the behaviour is mirror-like, but becomes progressively more banana-like above.

Fig. 4: *Analytic (1D) Airy last lobe fwhm Δr_{Ai^2} vs Δr of full-wave $|E^2|$, plus 2D empirical fit.*

5. Radial resolution

Fig. 4 shows the analytic Airy width vs the measured full-wave fwhm Δr from the $|E^2|$ map for the dataset. The generic

(O and X-mode) formula for the last Airy lobe fwhm is $\Delta r_{Ai2} = 0.478\, L_\epsilon^{1/3}\, \lambda_0^{2/3}$ where $L_\epsilon = (dN^2/dr)^{-1}$ is the permittivity gradient length [10] calculated from the density n_e and magnetic field B profiles along the radial through the ray turning point. For mirror conditions the agreement is good. However, the banana-like cases deviate significantly thus indicating 2D effects. These points (yellow) are empirically fitted by $\Delta r = 2(\Delta r_{Ai2})^2$ in units of cm. This 2D behaviour requires further theory and modelling [11].

6. Radial location

The beam/ray turning point (minimum ray N^2) corresponds well to the cutoff surface. Previously this was taken as the measurement location, however, 2D full-wave and Weighting function studies confirm the strongest response is from the W maximum, e.g. the last lobe radial position. Analytically, the distance between the cutoff and the last Airy lobe is given by $r_{Ai1} = 0.299\, L_\epsilon^{1/3}\, \lambda_0^{2/3}$ or, assuming the scaling of the peak displacment

Fig. 5: *Peak displacement r_d vs 1D analytic Airy last lobe distance r_{Ai1} for the database.*

and width holds, $r_{Ai1} = (0.299/0.478)\,\Delta r_{Ai2}$. Fig. 5 shows the full-wave $|E|^2$ peak displacement $r_d = (r_{pk} - r_{co})$ vs the Airy lobe r_{Ai1} for the dataset. The agreement with the 1D analytic is fairly good for the mirror points, but with growing deviation for the deep banana points. Replacing r_d with $(0.299/0.478)\,\Delta r$ gives similar trends as in fig. 4 but with a stronger 2D dependence for the banana points [11].
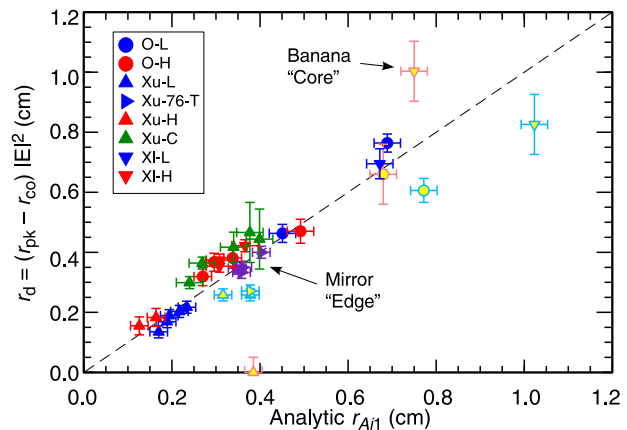
7. Peak wavenumber

Fig. 2(d) shows the wavenumber spectra at the cutoff layer and at the $|W|$ peak are not the same. In general, the ray trace $k_{\perp tp}$ at the ray turning point is close to the full-wave $k_{\perp co}$ at the cutoff, but can be significantly smaller than $k_{\perp pk}$ at the $|W|$ peak. The discrepancy grows with the peak to cutoff layer displacement $r_d = (r_{pk} - r_{co})$. Fig. 6 shows the wavenumber difference $k_d = (k_{\perp pk} - k_{\perp co})$ (along a flux surface path) vs the peak radial displacement r_d scaled from the

Fig. 6: *Perpendicular wavenumber difference k_d vs peak displacement r_d from W along flux path.*

fwhm Δr for $|W|$. The mirror points roughly fit an empirical scaling $k_d = 0.5\ln(r_d) + 1$ (rad/cm) with r_d in cm. For the banana points, $k_d \sim 0.8$ rad/cm is roughly constant.
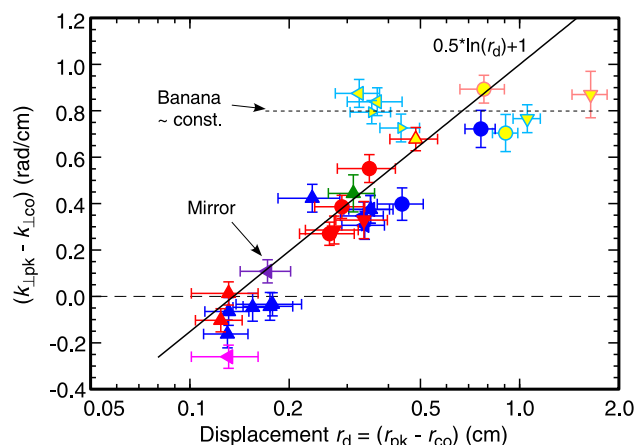
4

8. Wavenumber resolution

For flat cutoff layers, $R_{co} \to \infty$, and large beam phase-front radius, $R_b \to \infty$, the wavenumber peak width scales as $\Delta k_\perp \propto 2/T$. However, for finite curvatures Hirsch and Holzhauer [12] introduced an analytic formula based on vacuum Gaussian beams and the Weighting function width: $\delta k_\perp \propto w^{-1}[1 + w^4 k_0^2/\rho^2]^{1/2}$, where ρ is an effective curvature radius and w the $E_{1/e}$ beam radius at the cutoff. The full-wave database also follows the generic H&H model, but in a modified form: for the hwhm power $\Delta k_\perp/2 = \mathsf{w}^{-1}[1 + \mathsf{w}^4 k_0^2/(2\rho_{\mathrm{eff}}^2)]^{1/2}$, where $\rho_{\mathrm{eff}} = (2/(R_{co}\cos\theta) - 1/R_b)^{-1}$ for $w \ll R_{co}$ [13], with θ the beam LoS to cutoff-normal angle and $\mathsf{w} = w_{elip}\sqrt{\ln(2)/2}$ (of $|E|^2_{3\mathrm{dB}}$) with w_{elip} the projected spot $E_{1/e}$ radius. The coordinate system defines the sign of the cutoff (not flux) curvature radius $R_{co} > 0$ and beam $R_b < 0$. Both R_b and w are the vacuum beam values (as proposed by H&H) at the ray-tp path length, calculated using standard Gaussian beam equations.

Fig. 7 shows the $\Delta k_\perp/2$ from the model vs the W power spectra peak width. The model works for mirror cases but, as expected, breaks for banana cases as it is not appropriate for a beam propagating parallel to the cutoff. For the banana points $\Delta k/2 \sim 2/T_m$ where T_m is the interaction zone length calculable from the TORBEAM beam envelope with a curvature correction [11].
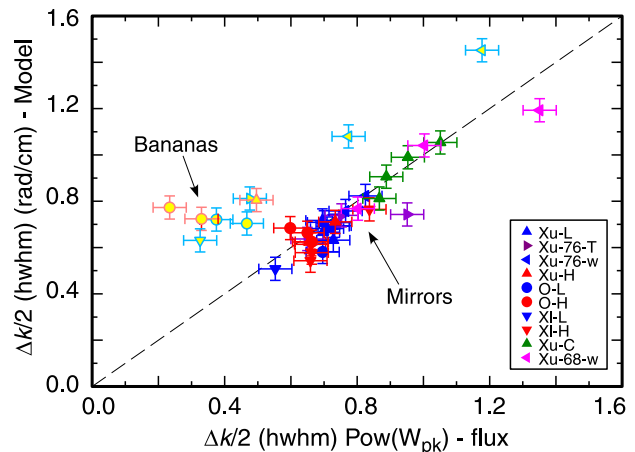

Fig. 7: *Wavenumber resolution (hwhm) $\Delta k_\perp/2$ from model vs full-wave hwhm $Pow(W_{pk})$ spectral peak width (flux surface path).*

9. Conclusions

Full-wave simulations reveal a transition in the Doppler refl. beam behaviour from a 1D (mirror-like: small tilt or steep/edge $\nabla_r k$) to a 2D (banana-path: large tilt or shallow/core $\nabla_r k$). The transition point is given by a simple Airy integral criterion. The principle backscatter radial location is also displaced from the cutoff (i.e. ray-trace tp) as given by the Airy last lobe distance r_{Ai1}. However, significant contributions to the backscatter can arise from the 2nd or 3rd to last lobe regions for very low L_ϵ mirror cases. The radial width is given by the Δr_{Ai^2} for mirror conditions, but 2D effects become important in banana conditions leading to a modified Δr dependence. The peak displacement means the ray-trace $k_{\perp tp}$ must also be corrected. Here, empirical formulas for mirror and banana cases are proposed. Concerning the wavenumber width, for mirror cases a modified H&H type model is appropriate, but is not appropriate for banana conditions where $\Delta k_\perp$ scales with the interaction zone perpendicular length as $2/T_m$. It must be stressed that the modelling results here represent ideal or minimal values. Additional effects due to the

5

turbulence itself, such as forward scattering, may lead to additional broadening of Δr and $\Delta k_\perp$. Nevertheless, some simple workable corrections to ray-trace values are given.

References

[1] G.D.Conway *et al.* Proc. 12th Int. Reflectometer Wksh. (Jülich) - IRW12 (2015).

[2] G.D.Conway *et al.* Plasma Phys. Control. Fusion **46**, 951 (2004).

[3] C.Lechte *et al.* Plasma Phys. Control. Fusion **59**, 075006 (2017).

[4] E.Poli *et al.* Comput. Phys. Commun. **136**, 90 (2001).

[5] E.Holzhauer *et al.* Plasma Phys. Control. Fusion **20**, 867 (1978).

[6] V.Bulanin & M.Yafanov, Plasma Phys. Rep. **32**, 47 (2006).

[7] I.H.Hutchinson, Plasma Phys. Control. Fusion **34**, 1225 (1992).

[8] E.Blanco *et al.* Plasma Phys. Control. Fusion **48**, 699 (2006).

[9] O.Maj *et al.* Plasma Phys. Control. Fusion **52**, 085006 (2010).

[10] R.Nazikian *et al.* Phys. Plasma **8**, 1840 (2001).

[11] G.D.Conway *et al.* To be submitted.

[12] M.Hirsch & E.Holzhauer, Plasma Phys. Control. Fusion **43**, 1641 (2001).

[13] E.Poli *et al.* Phys. Plasma **8**, 4325 (2001).